AzTEC 1.1 mm OBSERVATIONS OF THE MBM12 MOLECULAR CLOUD

M. J. Kim[1], S. Kim[1], S. Youn[1], M. S. Yun[2], G. W. Wilson[2], I. Aretxaga[3], J. P. Williams[4], D. H. Hughes[3], A. Humphrey[3],
J. E. Austermann[5], T. A. Perera[6], P. D. Mauskopf[7], L. Magnani[8], and Y.-W. Kang[1]

[1] Department of Astronomy & Space Science, Sejong University, KwangJin-gu, KunJa-dong 98, Seoul 143-747, Republic of Korea; sek@sejong.ac.kr
[2] Department of Astronomy, University of Massachusetts, 710 North Pleasant St., Amherst, MA 01003, USA
[3] Instituto Nacional de Astrofísca, Óptica y Electrónica, Tonantzintla, Puebla, Mexico
[4] Institute for Astronomy, University of Hawaii, 2680 Woodlawn Drive, Honolulu, HI 96822, USA
[5] Department of Astrophysical and Planetary Sciences, University of Colorado, Boulder, Colorado 80309, USA
[6] Department of Physics, Illinois Wesleyan University, Bloomington, IL 61701, USA
[7] School of Physics and Astronomy, Cardiff University, Cardiff CF24 3AA, UK
[8] Department of Physics and Astronomy, The University of Georgia, Athens, GA 30602-2451, USA
Received 2011 August 26; accepted 2011 November 2; published 2012 January 19

ABSTRACT

We present 1.1 mm observations of the dust continuum emission from the MBM12 high-latitude molecular cloud observed with the Astronomical Thermal Emission Camera (AzTEC) mounted on the James Clerk Maxwell Telescope on Mauna Kea, Hawaii. We surveyed 6.34 deg^2 centered on MBM12, making this the largest area that has ever been surveyed in this region with submillimeter and millimeter telescopes. Eight secure individual sources were detected with a signal-to-noise ratio of over 4.4. These eight AzTEC sources can be considered to be real astronomical objects compared to the other candidates based on calculations of the false detection rate. The distribution of the detected 1.1 mm sources or compact 1.1 mm peaks is spatially anti-correlated with that of the 100 μm emission and the ^{12}CO emission. We detected the 1.1 mm dust continuum emitting sources associated with two classical T Tauri stars, LkHα262 and LkHα264. Observations of spectral energy distributions (SEDs) indicate that LkHα262 is likely to be Class II (pre-main-sequence star), but there are also indications that it could be a late Class I (protostar). A flared disk and a bipolar cavity in the models of Class I sources lead to more complicated SEDs. From the present AzTEC observations of the MBM12 region, it appears that other sources detected with AzTEC are likely to be extragalactic and located behind MBM12. Some of these have radio counterparts and their star formation rates are derived from a fit of the SEDs to the photometric evolution of galaxies in which the effects of a dusty interstellar medium have been included.

Key words: galaxies: high-redshift – ISM: molecules – stars: pre-main sequence – stars: protostars – submillimeter: galaxies – submillimeter: stars

Online-only material: color figures

1. INTRODUCTION

The MBM12 molecular cloud was cataloged as L1453−L1454, L1457, and L1458 in Lynds' Dark Cloud Catalog (Lynds 1962) and is one of the nearby high-latitude molecular clouds (Magnani et al. 1985). Until recently, MBM12 was considered to be the nearest star-forming region; however, its distance has been revised to 275 pc by Luhman (2001) and at 360 ± 30 pc from the photometric and spectroscopic results of the Sloan Digital Sky Survey (SDSS) and the Two Micron All Sky Survey (2MASS; Andersson et al. 2002). Thus, although it is still nearby, it is farther out than the Taurus dark clouds and Ophiuchus star-forming regions.

A few young stars were reported in MBM12 (Hearty et al. 2000a; Hogerheijde et al. 2003) and their presence demonstrated that star formation had occurred recently in at least this particular high-latitude molecular cloud (Broeg et al. 2006). The high-latitude molecular clouds are known to be translucent, and the low-density environments found in high-latitude clouds create a challenge for star formation by gravitational collapse. The ability of at least a few high-latitude clouds to form cold molecular cores and young stars may be due to a combination of conditions, including variations in the interstellar radiation field, changes in dust-grain size and chemistry, and turbulence in the interstellar medium (ISM).

Regardless of the formation mechanisms, the study of high-latitude star formation environments continues to intrigue researchers, because it is difficult to see how star formation in the low-density environments found in typical high-latitude molecular clouds can proceed via direct gravitational collapse. High-latitude pre-main-sequence (PMS) stars found in isolation could be formed by ejection from their parent cloud or dissipation of the natal cloud. Dissipation timescales for these unbound clouds appear to be a few Myr. It is possible that outflows from low-mass stars that form in low-density environments can drive the dissipation of the parent cloud (Sterzik & Durisen 1995; Feigelson 1996).

In the present paper, we describe the results of our observations of the dust continuum emission from MBM12 at a wavelength of 1.1 mm observed with the AzTEC (Wilson et al. 2008) on the James Clerk Maxwell Telescope (JCMT). Dust continuum emission at (sub)millimeter wavelengths can identify the star-forming sites in the molecular clouds and determine the evolutionary stages of young stellar objects. In Section 2, we describe the observations and data reduction procedure. In Section 3, we present information on the sources detected at 1.1 mm and investigate their spectral energy distributions (SEDs). We also describe the assembly of the SEDs and the procedure used to fit the models, and how models were fitted to the data to determine the physical
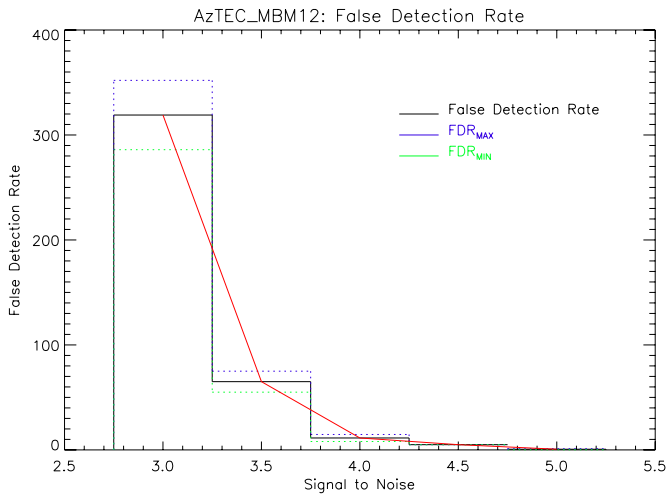
Figure 1. FDR at each threshold of 3σ–5σ, each step corresponds to 0.5σ.
(A color version of this figure is available in the online journal.)

Table 1
The Calculated FDR of the AzTEC Sources in the MBM12 Regions

Area	Signal ($>5\sigma$)	Average Noise rms (Jy beam^{-1})	FDR
A1	1	0.009	0.18 ± 0.10
A2	2	0.007	0.19 ± 0.81
A3	0	0.007	0
A4	2	0.011	0.36 ± 0.09
A9	1	0.013	0.64 ± 0.54

parameters of the detected sources from present observations. In Section 4, we summarize the results of our observations and analysis.

2. OBSERVATIONS AND DATA REDUCTION

Observations of MBM12 were performed in raster scan mode between 2005 November and 2006 January using AzTEC mounted on the JCMT. The beam size was 18 arcsec, and the scan velocity was 120 arcsec s^{-1}. AzTEC is a new bolometric array instrument and was developed for the Large Millimeter Telescope at the University of Massachusetts at Amherst (Wilson et al. 2008). This array camera consists of 144 Si$_3$N$_4$ micromesh bolometers and operates at 1.1 mm and 2.1 mm. In 2005, this bolometer array was tested by invitation at the JCMT on Mauna Kea in Hawaii. It is an appropriate instrument for surveys of Submillimeter Galaxies (SMGs) at low and high redshifts and searches for protostellar dusty cores in nearby molecular clouds. We surveyed about 6.34 deg^2 of the sky centered on R.A. = 02^h56^m0, decl. = 19^d30^m0 in J2000. This is the largest area centered on MBM12 that has ever been surveyed using continuum instruments in the submillimeter and millimeter parts of the spectrum. The area was covered with a total of 36 scan maps. Twenty-seven scans were retrieved and combined, covering a total observed area of 655.35 arcmin^2. The average rms was 9.695 mJy beam^{-1}. AzTEC suffered a pointing error of about $2''$. Beam maps were made from observations of Uranus with a mean flux density of 42.2 Jy at 1.1 mm during the JCMT observing run. A pointing model was generated using CRL618, a post-AGB (asymptotic giant branch) star with a mean flux density of 2.7 Jy at 1.1 mm. The intensity calibration errors were estimated to be $\pm6\%$–13% (Wilson et al. 2008). The raw bolometer array observations were calibrated and edited in the standard AzTEC IDL software (Scott et al. 2008; Austermann et al. 2010). The AzTEC instrument team has constructed data-reduction codes in the IDL language. Using the AzTEC software, we cleaned and co-added the array observations. To remove atmospheric signals, we adopted the principal component analysis (PCA) technique (Heyer & Schloerb 1997; Francis & Wills 1999), a tool for simplifying several parameters to clarify their relationships. Given a sample of n objects with p parameters, x_j ($j = 1, ..., p$), the orthogonal

variables, ξ_i ($i = 1, ..., p$), can be described as

$$\xi_i = a_{i1}x_1 + \cdots + a_{ij}x_j + \cdots + a_{ip}x_p. \quad (1)$$

The ξ_i represent the principal component, and the correlated and observed variables flag important principal components (Brunt & Heyer 2002). Hence, atmospheric signals with large spatial fluctuation show dominant principal components, whereas point signals such as distant galaxies do not. We adapted the PCA cleaning routine by constructing a covariance matrix from the $N_{\rm bolo} \times N_{\rm time}$ time-stream data (Scott et al. 2008; Austermann et al. 2010). To provide an eigenvalue decomposition on the matrix, we neglected the eigenfunctions corresponding to eigenvalues larger than 2.5σ as atmospheric effects (Scott et al. 2008; Austermann et al. 2010). To maximize the signal-to-noise ratio (S/N), the four cleaned raw data sets were co-added with the Wiener filter, $g(q)$, described as

$$g(q) = \frac{s^*(q)/J(q)}{\int |s(q)|^2/J(q)d^2q}, \quad (2)$$

where $s(q)$ is the Fourier transform of the beam shape from map space to spatial frequency space, q, and $J(q)$ implies the average power spectral densities (PSDs). Through filtering with the Wiener filter (Scott et al. 2008; Austermann et al. 2010) in Fourier space, the noise at low and high frequencies was effectively attenuated (Laurent et al. 2005). Using the Wiener filter and removing the PCA components reduces the rms noise per pixel, but the resolution of the optimally filtered map appeared to be the same. The peak brightness of point sources and compact peaks would be also preserved. However, after optimal filtering extended sources in the map will be trimmed to remove areas of low coverage (Enoch et al. 2007). The final image of MBM12 contains eight sources detected at a S/N of greater than 4.0σ (Figure 1). The average rms noise over the entire image is 2.71 mJy beam^{-1}. The catalog of the AzTEC mm source candidates is listed in Table 1. The flux values of the source candidates range from 10 ± 2.7 mJy to 12 ± 2.7 mJy.

We generated noise maps by randomly multiplying each scan in the cleaned time stream data by ±1 and co-adding (Perera et al. 2008; Scott et al. 2008). The sources were removed, and the random noises were accumulated in the co-added noise map (Austermann et al. 2010). We constructed 100 noise maps by iteration. We determined the false detection rate (FDR) by analyzing the noise properties of these maps by counting signals detected with a flux over a threshold in each noise map and then estimating the average detections (Perera et al. 2008). The FDR was defined as the source detections divided by the average false detections. The FDR at each threshold is shown in Figure 1. At over 3.0σ, 312 sources were detected, and the FDR was 319 ± 66. However, at over 4.4σ, eight sources were detected, and the FDR value was smaller than 1. Therefore, these eight AzTEC sources are more likely to be real astronomical objects than

Table 2
Observed AzTEC Sources in the MBM12 Region

Source		R.A. (J2000)	Decl. (J2000)	Flux (mJy beam^{-1})	S/N
A1$_1$	J0225+1904	02:55:17.3	19:04:48	45.6 ± 3.6	5.2
A2$_1$	J0256+2005 (LkHα262)	02:56:37.5	20:05:36	87.8 ± 7.0	12.6
A2$_2$	J0256+2003 (LkHα264)	02:56:07.7	20:03:24	44.9 ± 3.6	6.3
A3$_1$	J0258+2030	02:58:07.3	20:30:00	29.6 ± 2.4	4.4
A4$_1$	J0259+1925	02:59:29.5	19:25:42	234.3 ± 18.7	22.7
A4$_2$	J0258+1953	02:58:41.3	19:53:18	50.7 ± 4.0	5.0
A9$_1$	J0253+1805	02:53:34.8	18:05:42	298.5 ± 23.9	11.4
A9$_2$	J0257+1847	02:57:45.6	18:47:06	53.6 ± 4.2	4.4

Notes. Units of R.A. are in hours, minutes, and seconds. Units of decl. are in degrees, arcminutes, and arcseconds. The positional uncertainties of sources are likely to be of order of $1''$ in R.A. and decl..

the others. The results from the calculations of the FDR are summarized in Table 1.

3. RESULTS AND DISCUSSION

3.1. Distribution of the AzTEC 1.1 mm Dust Continuum Sources

Figure 2 presents the 1.1 mm dust continuum emitting AzTEC sources from the present AzTEC MBM12 survey. The ^{12}CO(1–0) contours from the AT&T Bell Lab, 7 m radio telescope survey of MBM12 (Pound et al. 1990) are shown overlaid on the *IRAS* 100 μm emission in Figure 3. It is clear from the figure that the ^{12}CO contours are spatially correlated with the 100 μm emission. The AzTEC 1.1 mm dust continuum sources appear to be spatially anti-correlated with the most intense ^{12}CO emitting region and, thus, with the more intense 100 μm *IRAS* regions in the cloud. The lack of AzTEC mm sources and compact peaks in the bright 100 μm emitting cores suggests that our AzTEC sources detected with the 1.1 mm bolometer camera trace a colder dust component in the region than the extragalactic sources. Figure 4 shows the 1.1 mm dust continuum AzTEC sources overlaid on the images of the 100 μm emission. The anti-correlation between the AzTEC dust continuum sources and the peaks of 100 μm *IRAS* and ^{12}CO(1–0) emission is clear from the figure.

3.2. Properties of the AzTEC Sources in the MBM12

We present eight AzTEC millimeter sources in Figure 2. These sources are overlaid on the *IRAS* 100 μm image in Figure 3. The catalog of detected sources is presented in Table 2. The sources in the catalog were detected with a S/N of over 4.4σ. Each point source is indicated on the co-added map of the MBM 12 region. The size of the circle in the box is 18 arcsec, which is the beam size of the AzTEC observations for the present survey. To identify the nature of these sources and their properties, we examined their SEDs. The intrinsic flux densities of the detected AzTEC sources were used for the analysis of their SEDs (Perera et al. 2008). Among the eight AzTEC sources, two sources (A2$_1$, A2$_2$) in Table 1 correspond to known T Tauri stars, LkHα 262 and LkHα 264, with strong Hα emission and Li I absorption (Hearty et al. 2000a; Luhman 2001). Studies of seven T Tauri stars in this region were conducted previously (Table 3).

Table 3
Previously Observed T Tauri Stars in the MBM12

Star	R.A. (J2000)	Decl. (J2000)	Ref.
RXJ0255.4+2005	02:55:25.7	20:04:53	6
LkHα 262	02:56:07.9	20:03:25	1, 2
LkHα 263	02:56:08.4	20:03:39	1, 2
LkHα 264	02:56:37.5	20:05:38	1, 2, 3, 4
E02553+2018	02:58:11.2	20:30:04	2, 5
RXJ0258.3+1947	02:58:15.9	19:47:17	6
RXJ0256.3+2005	02:56:17.9	20:06:10	6

Notes. Units of R.A. are in hours, minutes, and seconds. Units of decl. are in degrees, arcminutes, and arcseconds.
References. (1) Herbig & Bell 1988; (2) Fernández et al. 1995; (3) Magnani et al. 1995; (4) Gameiro et al. 1993; (5) Caillault et al. 1995; (6) Hearty et al. 2000a.

3.2.1. AzTEC Sources with Lower FDR

J0256+2005 (A2$_1$) and J0256+2003 (A2$_2$): we detected 1.1 mm dust continuum emitting sources associated with LkHα 262 (J0256+2005) and LkHα 264 (J0256+2003). Previous studies by Hogerheijde et al. (2003) reported observing continuum emission from the disks around the classical T Tauri stars LkHα 262, LkHα 263, and LkHα 264 at 450 μm and 850 μm with Submillimeter Common User Bolometer Array (SCUBA). These two stars, LkHα 262 and LkHα 264 (Itoh et al. 2003), emitting submillimeter and millimeter radiation, were reported as Class II (Hearty et al. 2000a; Luhman 2001; Hogerheijde et al. 2003). The SEDs in Figure 5 indicate that LkHα 262 is likely to be Class II, but there are also indications that this source might be a late Class I (André et al. 1993; Whitney et al. 2003) instead. The flux flattens toward the longer wavelengths, a phenomenon that can be seen in the late Class I. To provide a reasonable fit to the flux densities between 3.6 and 8.0 μm for the SED of LkHα 262, we used a one-dimensional radiative transfer model of DUSTY (Ivezic et al. 1999). The physical properties of the central source and the dusty envelope were derived from the modeling. The flux densities from the central source were absorbed by the dusty envelope and re-emitted to longer wavelengths. A dusty disk was considered in order to fit 24 μm and 70 μm wavelengths, since it was difficult to fit the flux densities using the stellar component. A power-law density distribution for the envelope was also tested for emission from the disk model. The estimated mass of the envelope was consistent with the mass of the envelope determined from the 1.1 mm continuum by fixing most of the free parameters. The
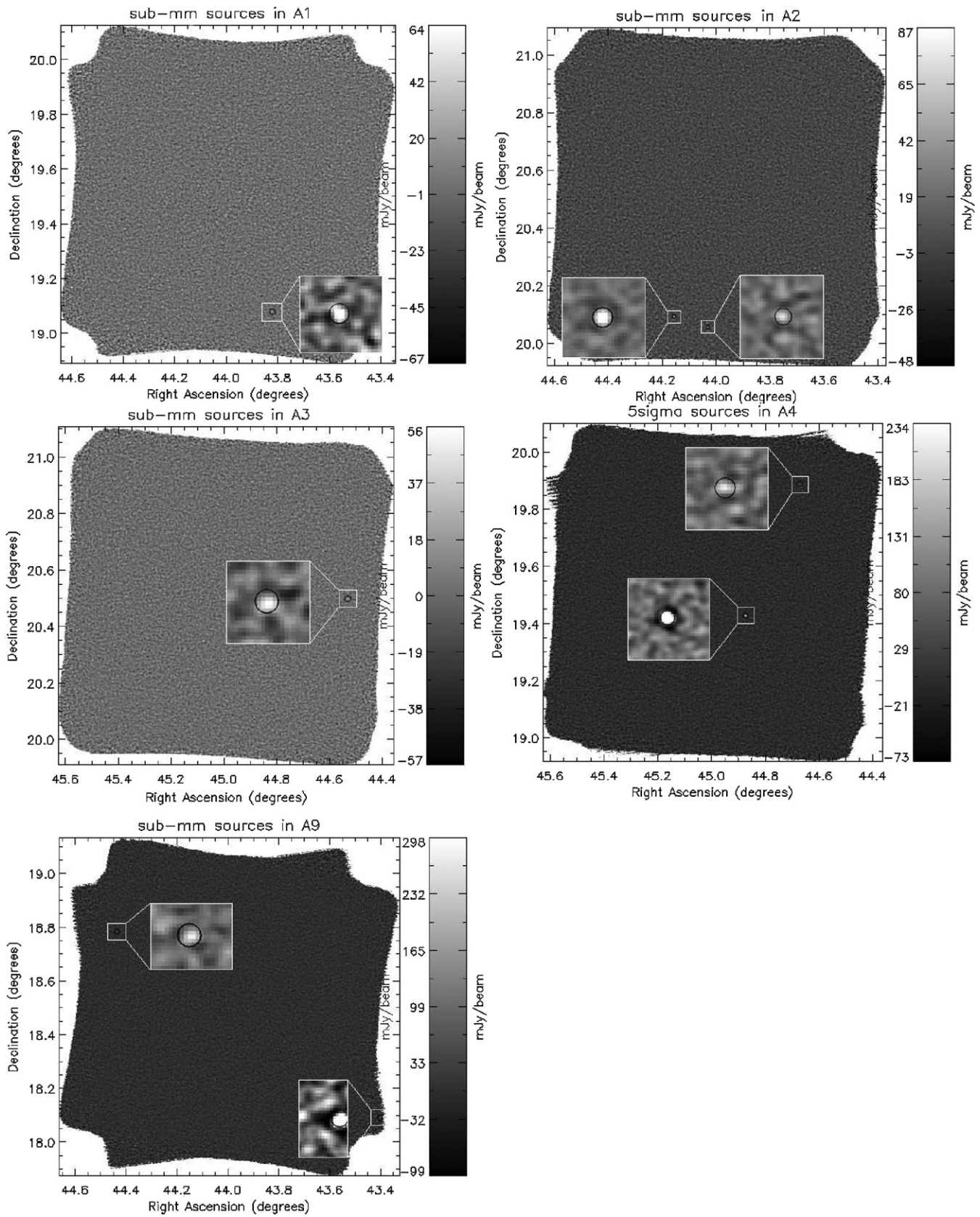
Figure 2. Eight AzTEC sources listed in Table 2 detected in the five regions covering the MBM12 high-latitude cloud.
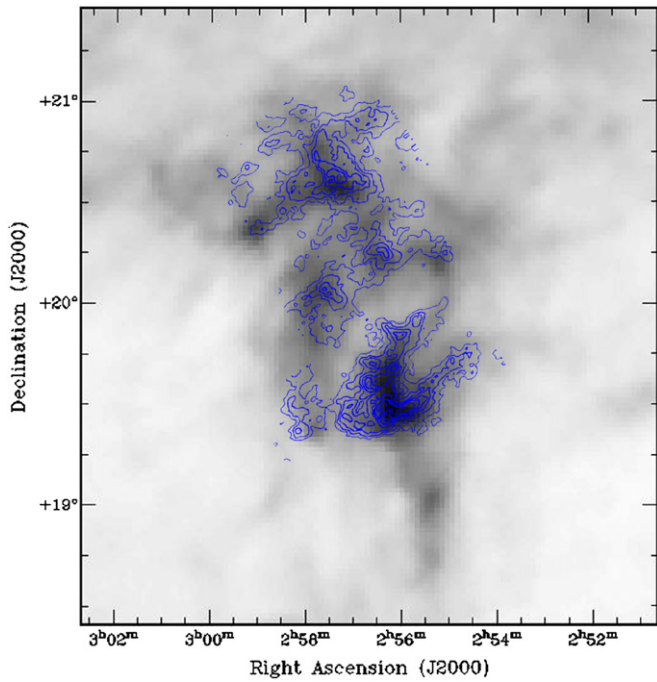
Figure 3. ^{12}CO contours from Pound et al. (1990) are overlaid on the *IRAS* 100 μm image of the MBM12 cloud.

Figure 4. Eight AzTEC sources listed in Table 2 overlaid on the *IRAS* 100 μm image.

mass of the envelope was determined from the flux density S at 1.1 mm, the Planck function at temperature T, and the dust opacity κ. The dust opacities used in this analysis were from OH5 dust in Ossenkopf & Henning (1994). The estimated mass was about 0.04 $M_\odot$ in the 15–20 K temperature range. Our detections might suggest that at least the disks of the classical T Tauri stars in MBM12 (1–5 Myr) have a mass range similar to the mass range of the disks of the younger ($\sim$1 Myr) Taurus and ρ Ophiuchus regions (0.001–0.3 $M_\odot$; Andrews & Williams 2007; Williams & Cieza 2011). Luhman (2001) argued that the near-IR K- and L-band excesses indicated that significant disk dispersal had occurred in MBM12.

3.2.2. AzTEC Sources with Higher FDR

RXJ0255.4+2005: this object was classified as a weak-line T Tauri star (WTTS). Its spectral type was labeled as K6 by Hearty et al. (2000b). T_{eff} was reported as 4205 K by Luhman (1999) and 4275 K by Hearty et al. (2000b). Hogerheijde et al. (2002) calculated the disk mass and diameter using the Owens Valley Radio Observatory (OVRO) to observe the $\lambda = 3$ mm continuum. The results were reported as 0.04 $M_\odot$ and 52 AU, respectively. These values were based on a distance of 275 pc and a gas-to-dust ratio of 100. The disk mass could be 0.023 $M_\odot$ at the distance of 360 pc. There were also studies by Hearty et al. (2000b) and Herbst et al. (2004) for the line widths of Hα from the source. The emission line widths were -1.26 Å (Hearty et al. 2000b) and -1.1 Å (Herbst et al. 2004). The flux of this object varies, and the period was reported as 6.22 days by Herbst et al. (2004) and 3.36 $\pm$ 0.17 days by Broeg et al. (2006).

E02553+2018: this object appears on the border between a classical and a WTTS. The emission line width of Hα is about -1.6 Å (Hearty et al. 2000b) and -2.5 Å (Herbst et al. 2004). Its spectral type is K3 (Fleming et al. 1989) or K4 (Hearty et al. 2000b). The effective temperature, T_{eff}, of this object is 4660 K as calculated by Luhman (1999) and 4593 K by Hearty et al. (2000b). Hogerheijde et al. (2002) obtained a disk mass
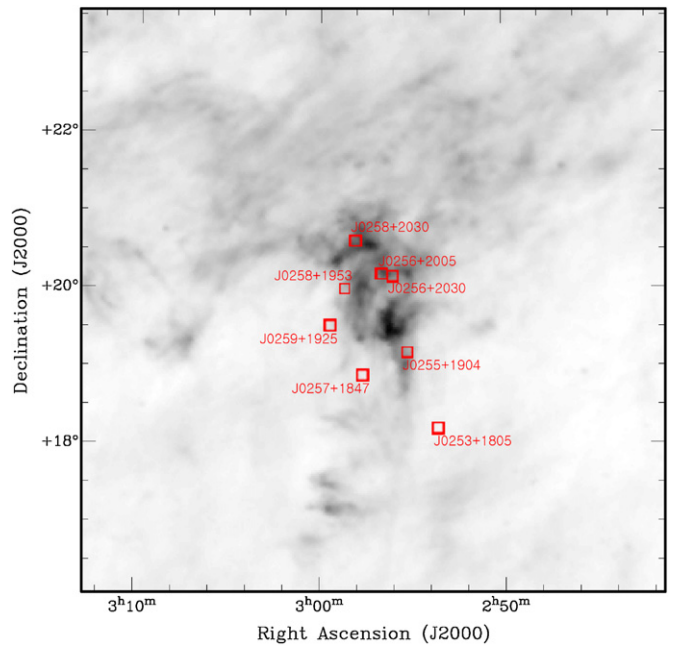
of 0.07 $M_\odot$ and a diameter of 66 AU. The flux was measured as 11 mJy with OVRO. The disk mass could be 0.04 $M_\odot$ at the distance of 360 pc. This object has an additional component of $V_{\text{LSR}} = -1.5$ km s^{-1}.

RXJ0258.3+1947: this object was classified as a classical T Tauri star (CTTS). Its spectral type was determined as M5 (Hearty et al. 2000b) or M4.5 (Luhman 2001). The effective temperature, T_{eff}, was calculated as 3198 K by Luhman (1999) and 3169 K by Hearty et al. (2000b). The flux at 3 mm was 5 mJy and the disk mass was 0.05 $M_\odot$. The disk mass could be 0.03 $M_\odot$ at the distance of 360 pc. Its diameter was 58 AU from OVRO observations, and JCMT observations yielded a mass of $8 \times 10^{-4} M_\odot$ (Hogerheijde et al. 2002). Its flux varies, and the period was reported as 1.205 days (Herbst et al. 2004). This was confirmed with reports of an Hα emission line width of -24.5 Å from Hearty et al. (2000b) and $-25 \sim -34$ Å from Herbst et al. (2004).

RXJ0256.3+2005: this object was classified as a WTTS and is the latest spectral type in the field of MBM12. Its spectral type was designated as M5.75 (Luhman 2001) and M6 (Herbst et al. 2004). Luhman (1999) calculated that the effective temperature, T_{eff}, was 3024 K. The mass was between 0.15 and 0.1 $M_\odot$ (Meeus et al. 2009). Its Hα emission line width was -13.5 Å (Herbst et al. 2004).

3.3. Properties of the AzTEC Sources behind the MBM12

From the present AzTEC observations of the MBM12 region, we find that other detected sources are likely to be located behind MBM12. Four AzTEC objects, defined as J0258+2030 (A3$_1$), J0259+1925 (A4$_1$), J0253+1805 (A9$_1$), and J0257+1847 (A9$_2$), were previously studied in the 1.4 GHz NRAO VLA survey for the sky of $\delta \geqslant -40°$ in J2000 (Condon et al. 1998). J0259+1925 (A4$_1$) is known as quasi-stellar object (QSO) at a redshift of $z = 0.54$. The flux density of this object at 1.4 GHz was 169.9 mJy. Three AzTEC sources, J0258+2030 (A3$_1$), J0253+1805 (A9$_1$), and J0257+1847 (A9$_2$), have radio counterparts observed by Condon et al. (1998) with the VLA at
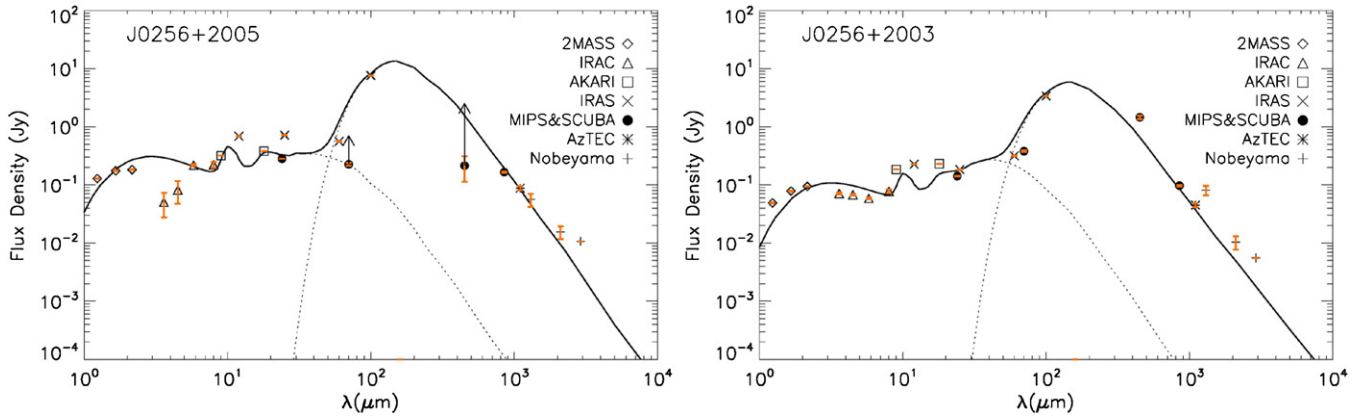
Figure 5. SEDs of two AzTEC sources corresponding to the candidates of protostars, J0256 + 2005 (left) and J0256 + 2003 (right).
(A color version of this figure is available in the online journal.)

Table 4
Fluxes at Other Wavelengths for the Detected AzTEC Sources

Source	2MASS $J(1.25\,\mu m)$ (mJy)	2MASS $H(1.65\,\mu m)$ (mJy)	2MASS $K(2.17\,\mu m)$ (mJy)	$S_{1.4\,GHz}$ (mJy)	z	Ref.
J0255+1904	$(<)\,6.05 \pm 0.097$	$(<)\,18.0 \pm 0.306$	$(<)\,21.3 \pm 0.341$			
J0256+2005	129.0 ± 2.064	175.0 ± 2.975	183.0 ± 1.994			1, 2, 6, 8
J0256+2003	49.0 ± 0.784	78.5 ± 1.335	94.6 ± 1.031			1, 5, 6, 7
J0258+2030	0.663 ± 0.097	1.04 ± 0.067	1.62 ± 0.08	98.1 ± 3.0		2, 3
J0259+1925	$(<)\,6.05 \pm 0.097$	$(<)\,18.0 \pm 0.306$	$(<)\,21.3 \pm 0.341$	163.7 ± 4.9	0.54	2, 9
J0258+1953	$(<)\,6.05 \pm 0.097$	$(<)\,18.0 \pm 0.306$	$(<)\,21.3 \pm 0.341$	98.1 ± 3.0		
J0253+1805	$(<)\,6.05 \pm 0.097$	$(<)\,18.0 \pm 0.306$	$(<)\,21.3 \pm 0.341$	304.0 ± 9.1	0.427	2, 4, 10
J0257+1847	$(<)\,6.05 \pm 0.097$	$(<)\,18.0 \pm 0.306$	$(<)\,21.3 \pm 0.341$	103.7 ± 3.1		2, 3, 4, 11

References. (1) Cutri et al. 2003; (2) Condon et al. 1998; (3) Gregory et al. 1996; (4) Snellen et al. 2002; (5) Herbig & Bell 1988; (6) Fernández et al. 1995; (7) Magnani et al. 1995; (8) Gameiro et al. 1993; (9) Caccianiga et al. 2000; (10) Ma et al. 1998; (11) Beasley et al. 2002.

1.4 GHz. The counterpart corresponding to J0259+1925 (A4$_1$) was also classified as J025929+1925.7 (1REX) in the radio emitting X-ray sources (REXs) survey by Caccianiga et al. (2000). Its X-ray flux was reported as 2.34×10^{-13} erg s^{-1} cm^{-2}. The NRAO VLA Sky Survey (NVSS) position of this source suggests that this object should be $\alpha = 02^h59^m29{.}^s65$, $\delta = +19°25'44{.}''9$ (J2000) at radio wavelengths. From the present AzTEC observations, the position of J0259+1925 was measured as $\alpha = 02^h59^m29{.}^s5$, $\delta = +19°25'42''$ at millimeter wavelengths. So the difference between the radio and millimeter emission is $\Delta\alpha = 0{.}^s15$ and $\Delta\delta = 2{.}''9$. The flux at 1.1mm measured with AzTEC was 234.3 mJy beam^{-1}. The AzTEC source A9$_1$ corresponds to J0253+1805 (J2000) in the NRAO VLA sky survey at 1.4 GHz (Condon et al. 1998). The coordinate of J0253+1805 (A9$_1$) was reported as $\alpha = 02^h53^m34{.}^s88$, $\delta = +18°05'42{.}''53$ (J2000) using the VLA observations. This position agrees with the identification by the Automated Plate Measurement (APM) Facility at Cambridge of the radio sources from the Jodrell Bank VLA Astrometric Survey (JVAS) (Snellen et al. 2002). We also compared the fluxes at 6 mm (Green Bank), NVSS 1.4 GHz (NRAO VLA Sky Survey), Green Bank 1.4 GHz, and VLA 1.4 GHz. The results were, respectively, 248, 304, 426, and 154 mJy. The millimeter-wavelength flux from this study was 298.5 mJy beam^{-1} at 1.1 mm. The AzTEC source detected as J0257+1847 (A9$_2$) has its counterpart in the radio source in the NRAO VLA sky survey by Condon et al.

(1998). This source was also included in the Very Long Baseline Array (VLBA) Calibrator Survey (VCS1) at 2.3 and 8.4 GHz (Beasley et al. 2002). Snellen et al. (2002) also obtained the flux densities of this object at 6 mm (Green Bank), 1.4 GHz (NVSS), 1.4 GHz (Green Bank), and 1.4 GHz (VLA) as 209, 103, 180, and 241 mJy, respectively. Synchrotron properties and the spectral indices of these objects will be discussed in detail in a future paper (S. Kim et al., in preparation). The coordinates of the AzTEC source agree to within $\alpha = 02^h57^m45{.}^s6$, $\delta = +18°47'06''$ (J2000). The flux at 1.1 mm is 53.6 mJy beam^{-1}. The fluxes at other wavelengths were compared in the SEDs presented in Figure 6. Although two AzTEC sources, J0225+1904 (A1$_1$) and J0258+1953 (A4$_2$), do not have counterparts at other wavelengths, we also performed a stacking analysis (Scott et al. 2008) on these AzTEC detections to calculate upper limits of the fluxes at the near-infrared images (Table 4). The GRASIL model (Silva et al. 1998) computes the photometric evolution of galaxies based on the SEDs of the AzTEC sources, including the effects of a dusty interstellar medium. The model includes the escape time of young stars from molecular clouds, the fraction of residual gas in molecular clouds, the radius of molecular clouds, etc. The star formation rate (SFR) could be also derived by fitting the SEDs to the model (Kim et al. 2010). The results suggest that J0258+2030 (A3$_1$), J0253+1805 (A9$_1$), and J0257+1847 (A9$_2$) can have SFRs of 3.6×10^3 $M_\odot$ yr^{-1}, 3.3×10^4 $M_\odot$ yr^{-1}, and 2.9×10^2 $M_\odot$ yr^{-1},
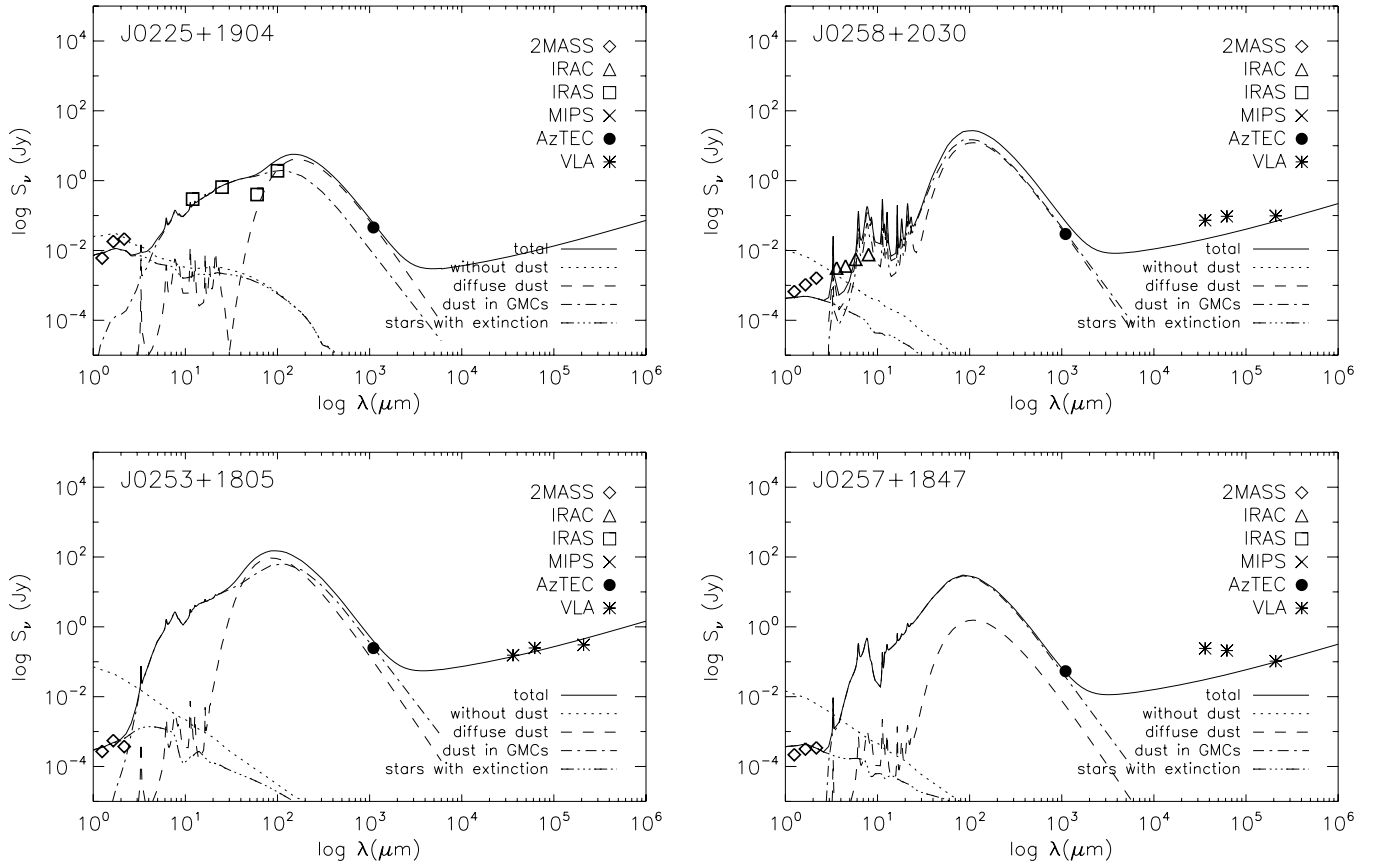
Figure 6. SEDs of four AzTEC sources corresponding to the candidates of extragalactic and submillimeter galaxies, J0225+1904 (top left), J0258+2030 (top right), J0253+1805 (bottom left), and J0257+1847 (bottom right).

respectively. The SFRs are similar to those studied in 16 radio galaxies with AzTEC counterparts in the far-IR and a graybody emission template with an emissivity index, β, and a dust temperature, T_d (Humphrey et al. 2011).

4. CONCLUSION

We presented observations of the dust continuum emission at 1.1 mm from MBM12 performed with AzTEC at the JCMT. We surveyed about 6.34 deg^2 field of sky. This is the largest area that has ever been surveyed for the MBM12 region with a (sub-)millimeter telescope. The distribution of 1.1 mm AzTEC sources is spatially anti-correlated with that of the 100 μm emission and that of the ^{12}CO emission. We detected 312 sources with a S/N of over 3σ. The FDR was 319 ± 66. Eight sources were detected with a S/N $> 4.4\sigma$ and with FDR value smaller than 1. These eight AzTEC sources can be considered to be real astronomical objects as opposed to spurious detections. We detected 1.1 mm sources associated with two classical T Tauri stars, LkHα262 and LkHα264. Observations of their SEDs indicate that LkHα262 is likely to be Class II but may be a late Class I. A flared disk and a bipolar cavity in models of Class I sources lead to more complicated SEDs. Our detections suggest that at least the classical T Tauri stars in MBM12 have disks in a similar mass range to the disks of stars in the Taurus or ρ Ophiuchus regions. From the present AzTEC observations of the MBM12 region, we find that some of the other detected sources are likely to be located behind the MBM12 molecular cloud. These have radio counterparts, and their SFRs were derived from fits of their SEDs to the photometric evolution of galaxies when

the effects of a dusty interstellar medium were included. These SFRs ranged from a few hundred to a few thousand $M_\odot$ yr^{-1}. Direct measurements of their redshifts should be performed with the Large Millimeter Telescope in the near future.

REFERENCES

Andersson, B.-G., Idzi, R., Uomoto, A., et al. 2002, AJ, 124, 2164
André, P., Ward-Thompson, D., & Barsony, M. 1993, ApJ, 406, 122
Andrews, S. M., & Williams, J. P. 2007, ApJ, 671, 1800
Austermann, J. E., Dunlop, J. S., Perera, T. A., et al. 2010, MNRAS, 401, 160
Beasley, A. J., Gordon, D., Peck, A. B., et al. 2002, ApJ, 141, 13
Broeg, C., Joergens, V., Fernández, M., et al. 2006, A&A, 450, 1135
Brunt, C. M., & Heyer, M. H. 2002, ApJ, 566, 276
Caccianiga, A., Maccacaro, T., Wolter, A., Della Ceca, R., & Gioia, I. M. 2000, A&A, 114, 247
Caillault, J.-P., Magnani, L., & Fryer, C. 1995, ApJ, 441, 261
Condon, J. J., Cotton, W. D., Greisen, E. W., et al. 1998, AJ, 115, 1693
Cutri, R. M., Skrutskie, M. F., van Dyk, S., et al. 2003, The IRSA 2MASS All-Sky Point Source Catalog, NASA/IPAC Infrared Science Archive
Enoch, M. L., Glenn, J., Evans, N. J., II, et al. 2007, ApJ, 666, 982
Feigelson, E. D. 1996, ApJ, 468, 306
Fernández, M., Ortiz, E., Eiroa, C., & Miranda, L. F. 1995, A&AS, 114, 439
Fleming, T. A., Gioia, I. M., & Maccacaro, T. 1989, ApJ, 340, 1011
Francis, P. J., & Wills, B. J. 1999, in ASP Conf. Ser. 162, Quasars and Cosmology, ed. G. Ferland & J. Baldwin (San Francisco, CA: ASP), 363
Gameiro, J. F., Lago, M. T. V. T., Lima, N. M., & Cameron, A. C. 1993, MNRAS, 261, 11
Gregory, P. C., Scott, W. K., Douglas, K., & Condon, J. J. 1996, ApJS, 103, 427
Hearty, T., Fernández, M., Alcalá, J. M., et al. 2000b, A&A, 357, 681
Hearty, T., Neuhäuser, R., Stelzer, B., et al. 2000a, A&A, 353, 1044
Herbig, G. H., & Bell, K. R. 1988, Lick Observatory Bulletin, IIII, 1
Herbst, W., Williams, E. C., & Hawley, W. P. 2004, AJ, 127, 1594
Heyer, M. H., & Schloerb, F. P. 1997, ApJ, 475, 173
Hogerheijde, M. R., Jayawardhana, R., Johnstone, D., Blake, G. A., & Kessler, J. E. 2002, AJ, 124, 3387
Hogerheijde, M. R., Johnstone, D., Matsuyama, I., Jayawardhana, R., & Muzerolle, J. 2003, ApJ, 593, L101
Humphrey, A., Zeballos, M., Aretxaga, I., et al. 2011, MNRAS, 418, 74
Itoh, Y., Sugitani, K., Fukuda, N., et al. 2003, ApJ, 586, 141
Ivezic, Z., Nenkova, M., & Elitzur, M. 1999, User Manual for DUSTY, University of Kentucky Internal Report (arXiv:astro-ph/9910475)
Kim, S., Kwon, E., Madden, S. C., et al. 2010, A&A, 518, 75
Laurent, G. T., Aguirre, J. E., Glenn, J., et al. 2005, ApJ, 623, 742
Luhman, K. L. 1999, ApJ, 525, 466
Luhman, K. L. 2001, ApJ, 560, 287
Lynds, B. T. 1962, ApJS, 7, 1
Ma, C., Arias, E. F., Eubanks, T. M., et al. 1998, AJ, 116, 516
Magnani, L., Blitz, L., & Mundy, L. 1985, ApJ, 295, 402
Magnani, L., Caillault, J.-P., Buchalter, A., & Beichman, C. A. 1995, ApJS, 96, 159
Meeus, G., Juhász, A., Henning, Th., et al. 2009, A&A, 497, 379
Ossenkopf, V., & Henning, Th. 1994, A&A, 291, 943
Perera, T. A., Chapin, E. L., Austermann, J. E., et al. 2008, MNRAS, 391, 1227
Pound, M. W., Wilson, R. W., & Bania, T. M. 1990, ApJ, 351, 165
Scott, K. S., Austermann, J. E., Perera, T. A., et al. 2008, MNRAS, 385, 2225
Silva, L., Granato, G. L., Bressan, A., & Danese, L. 1998, ApJ, 509, 103
Snellen, A. G., McMahon, R. G., Hook, I. M., & Browne, I. W. 2002, MNRAS, 329, 700
Sterzik, M. F., & Durisen, R. H. 1995, A&A, 304, L9
Whitney, B. A., Wood, K., Bjorkman, J. E., & Cohen, M. 2003, ApJ, 598, 1079
Williams, J. P., & Cieza, L. A. 2011, ARA&A, 49, 67
Wilson, G. W., Austermann, J. E., Perera, T. A., et al. 2008, MNRAS, 386, 807